ACS Catalysis

Research Article

pubs.acs.org/acscatalysis

Reaction Conditions of Methane-to-Methanol Conversion Affect the Structure of Active Copper Sites

Evalyn Mae C. Alayon,[†,‡] Maarten Nachtegaal,[†] Andras Bodi,[†] and Jeroen A. van Bokhoven*[,†,‡]

[†]Paul Scherrer Institut, CH-5232 Villigen, Switzerland

[‡]ETH Zurich, Wolfgang-Pauli-Strasse 10, CH-8093 Zurich, Switzerland

Supporting Information

ABSTRACT: Determining the structure of the active Cu sites, which are associated with the methane conversion intermediate during stepwise, low-temperature, methane-to-methanol conversion, represents an important step for the upgrade of this reaction route to a viable process. Quick X-ray absorption spectroscopy allowed us to follow the electronic and structural changes to the active Cu sites during reaction with methane and during desorption of the activated intermediate. A large fraction (41%) of the oxygen-activated Cu^{II} reacted with methane and underwent reduction to Cu^{I}. When the intermediate was released as the product MeOH into the gas phase after reaction with water, the fraction of Cu^{I} was simultaneously converted back to Cu^{II}. Therefore, the activation of methane involves a change in the copper oxidation state. Density functional theory calculations identified $[Cu^{I}-OCH_3-Cu^{II}]$ and $[Cu^{I}-OH-Cu^{II}]$ as energetically plausible structures of the adsorbed intermediates. The structure of the active Cu sites is also a function of conditions. In a dry pretreatment environment, the Cu sites took the form of dehydrated Cu^{II} oxide species, well characterized in the literature as mono(μ-oxo) and bis(μ-oxo)dicopper species. Under wet conditions, the dicopper species was destabilized to a hydrated Cu^{II} species, but a small amount of water-stable Cu^{II} oxide remained that was also active for conversion of methane to methanol.

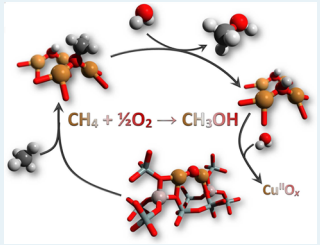

KEYWORDS: *quick X-ray absorption spectroscopy, Cu-mordenite, active site structure, methane, methanol*

INTRODUCTION

Developing a feasible process route for the low-temperature partial oxidation of methane to methanol is a necessary undertaking because of its potential to provide an inexpensive raw material for synthesis of chemicals, but it also poses challenges.[1] When Groothaert and co-workers discovered the ability of Cu-exchanged zeolites to convert methane to methanol at mild conditions (130−200 °C, ambient pressure) using molecular oxygen as the oxidant,[2] it inspired investigations into the reaction mechanism[3] and the active site structure.[4,5a] Recently, an Fe-based zeolite showed catalytic formation of methanol from methane in aqueous hydrogen peroxide.[5b] Identifying the active site and understanding the reaction mechanism are required to improve this reaction route to a considerably more feasible process. Woertink and co-workers[4a] used resonant Raman spectroscopy and density functional theory (DFT) calculations on a Cu-zeolite to identify the structure of the active site as a mono(μ-oxo)dicopper species. They proposed that, after oxygen activation, a cupric oxyl radical intermediate is formed that is capable of hydrogen abstraction from methane. Using DFT, Kurnaz and co-workers[6] studied C−H bond activation of methane on a M−O−M (M = Au, Ag, Fe, and Cu) bridge site on ZSM-5 and suggested the formation of an O−H bond at the oxygen bridge of the Cu−O−Cu site and a CH_3 radical in the gas phase, instead. More comprehensive discussions on methane activation are presented in recent reviews.[1b,7] These methane activation studies are encouraged by recent findings showing that the active Cu centers in Cu-zeolites share structural characteristics with the active centers found in the particulate methane monooxygenase enzyme in methanotrophic bacteria, which convert methane to methanol at their ambient living conditions.[8]

To date, a true catalytic methane-to-methanol conversion process at low temperature on Cu-zeolites remains unattained. Offline extraction was necessary because the intermediate formed after methane activation remains strongly sorbed on the zeolite.[2a,4b] Based on the amount of extracted methanol and the premise of a single dicopper complex reacting with one molecule of methane, only around 5% of the total Cu sites in Cu-ZSM-5 were proposed to be active.[2] Recently, we showed that interaction of the reacted methane with a wet gaseous stream released methanol, enabling batchwise operation.[5a] The exact nature of the sorbed, activated methane intermediate remains unknown. The DFT calculations by Woertink and co-workers showed that the formation of the supposed $[Cu^{I}-OHCH_3-Cu^{II}]$ intermediate from methane is endothermic by 13.8 kcal mol^{-1}.[4a,9] In our view, the high energy of this structure makes it unlikely that it is a bound intermediate in the process.

X-ray absorption spectroscopy (XAS) at the Cu K edge provides the local electronic and geometric structure specific to the Cu sites. The use of hard X-rays in XAS allows in situ measurements[10] to monitor the structure of all Cu sites during

Received: August 21, 2013
Revised: November 18, 2013
Published: November 20, 2013

   dx.doi.org/10.1021/cs400713c | ACS Catal. 2014, 4, 16−22

Scheme 1. Schematic Diagram of the Treatments on Cu−MOR for Methane-to-Methanol Conversion[a]

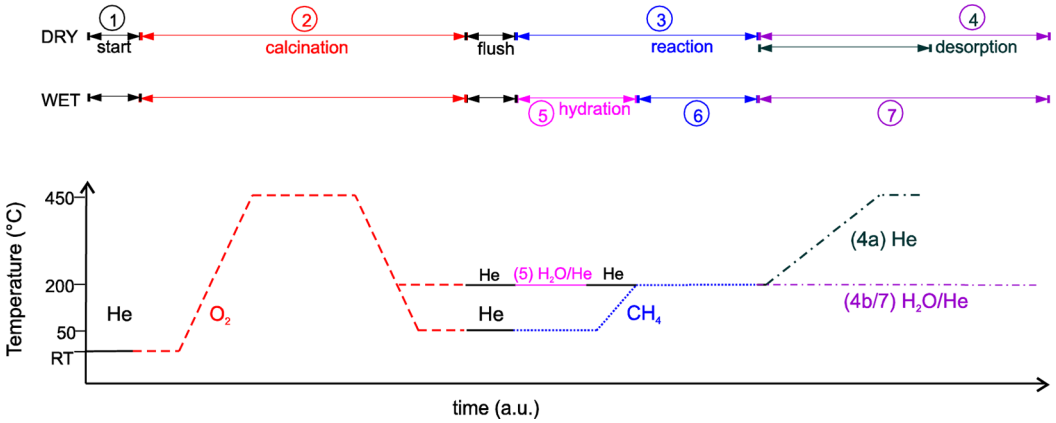

[a]Cu−MOR after ion exchange synthesis and drying (1) is calcined in oxygen at 450 °C to activate the copper sites (2). The activated Cu−MOR is cooled to 50 °C in flowing oxygen, and thereafter, helium is introduced briefly to remove the excess gas-phase oxygen. Methane is introduced, and the catalyst bed is heated to 200 °C for the reaction (3). The methane conversion intermediate is removed either by (4a) heating in dry helium flow or (4b) interaction with a wet stream of helium at 200 °C. In the wet treatment alternative, Cu−MOR after calcination is treated with a wet helium stream at 200 °C (5) to hydrate the activated Cu sites. The excess moisture in the catalyst bed and in the gas lines is removed with a short flush of helium. Subsequently, methane is introduced (6), and the methane conversion product is removed by interaction with a wet stream of helium (7). The encircled numbers correspond to the schematic description in Scheme 2.

the reaction. In a previous publication, we reported conventional transmission XAS and high-energy-fluorescence-detected XAS[11] data taken of Cu−MOR during methane-to-methanol conversion under steady state conditions and showed that about half of the total Cu sites have changed oxidation state after the methane activation step.[4c] In this contribution, we used quick XAS[10,12] with a time resolution of about 5 seconds to follow the changes to the Cu sites during reaction with methane and desorption of the activated intermediate. The desorption of the activated methane intermediate as MeOH occurs in the first few minutes from the instant that water is introduced. Therefore, it is the first few minutes of desorption that is relevant for observing the Cu species associated with the reaction pathway. After desorption of MeOH, we expect to observe changes to the coordination of Cu sites, which are associated only with further hydration. In addition to quick XAS to follow the electronic and geometric structural changes to the Cu sites, we used DFT to identify plausible stable structures of the adsorbed intermediates. Together with the identification of the nature of the active Cu sites, this contribution will yield new strategies for the development of a cyclic operated process.

EXPERIMENTAL SECTION

Cu−MOR was synthesized by aqueous ion exchange from copper acetate and the sodium form of mordenite. The synthesis and characterization steps are described in detail in a previous publication.[5a] The Si/Al ratio of the Na−MOR is 11 (ZeoChem). Cu elemental analysis indicated a Cu loading of 4.3%, which corresponds to a Cu/Al ratio of 0.38.

Quick XAS measurements were performed at the SuperXAS beamline, Swiss Light Source of the Paul Scherrer Institute in Villigen, Switzerland. Around 15 mg (250−500 μm sieve fraction) of Cu−MOR was placed in a 3 mm diameter, thin-walled (0.1 mm) quartz capillary. This resulted in an edge jump of ~0.5 of the transmission XAS spectra. The material was held in place by quartz wool. The capillary was heated by a hot air blower. Gas flows were controlled by mass flow controllers in a setup that allows gas mixing and switching. All gas lines were heated to 110 °C to prevent condensation. A water bubbler in the setup, containing deionized water, allowed saturation of He with water at room temperature. A quadrupole mass spectrometer (MS, Omnistar GSD 300 O2 from Pfeiffer Vacuum) was attached to the exhaust line to monitor the composition of the gas stream that was going out of the catalyst bed. Cu−MOR was heated at 1 °C/min to 450 °C in 50 mL/min pure O_2 (quality 5.0) and calcined for 4 h at 450 °C. After calcination, it was cooled to 50 °C at 5 °C/min in O_2 flow. The excess gas phase oxygen was removed by a 10 min, 30 mL/min flow of He (quality 5.0) containing 1 ppmv O_2 and 3 ppmv H_2O called He(O_2). The gas flow was switched to a 5 vol % CH_4/He feed (quality 4.5 CH_4 in 5.0 He) at 30 mL/min, and the catalyst bed was heated at 10 °C/min to 200 °C for a 30 min methane interaction. For desorption in dry feed, the methane-reacted Cu−MOR was heated from 200 to 450 °C at 5 °C/min in 30 mL/min dry He(O_2). For desorption in wet feed, the methane-reacted Cu−MOR was allowed to interact with a 30 mL/min stream of water-saturated helium for 30 min. At each reaction step, in situ XAS spectra were collected in transmission mode using a channel-cut Si-111 monochromator oscillating at a frequency of 0.1 Hz, resulting in 2 spectra per 10 s and covering about 600 eV per spectrum.[12] Cu foil spectra were collected simultaneously for internal energy calibration (edge energy, E_0 = 8979 eV).

Standard XAS data reduction steps were performed with XDAP.[13] These include subtraction of pre-edge and postedge backgrounds, determination of the edge energy, and normalization of the data set to an edge jump of 1. Linear combination fitting (LCF) of the X-ray absorption near edge structure (XANES) region of each normalized XAS spectrum was performed with the Athena program of the Iffeffit software package over a range of −20 to 50 eV around the absorption edge.[14] The spectra recorded of Cu−MOR after ion exchange, after calcination at 450 °C, after hydrogen treatment at 200 °C, and after hydrogen treatment at 500 °C to represent the Cu species in Cu−MOR in the fully hydrated, fully oxidized Cu^{II}, reduced Cu^{I}, and fully reduced Cu^{0} states, respectively, were used as standards in the LCF. The similarities of the Cu−MOR

dx.doi.org/10.1021/cs400713c | ACS Catal. 2014, 4, 16−22

spectra to the XANES spectra of copper compounds, such as copper(II) hydroxide, copper(II) oxide, copper(I) oxide, and metallic copper, in terms of oxidation state but differences in terms of long-range geometric order, as seen in the Fourier transform (FT) of the extended X-ray absorption fine structure (EXAFS) spectra, are motivations for their use as LCF input structures for fitting the XANES region. Further details on these input structures for fitting are presented in the Supporting Information (SI) (Figures S1 and S2). The sum of the weights of the standards during LCF of the XANES was constrained to 1.

Unrestricted DFT calculations were performed using Gaussian 09[15] with the B3LYP and M06-2X functionals and the 6-311+G(d) and def2-TZVP basis sets, respectively, on a Cu-ZSM-5 model[4a] for easy comparison with previous results. The triplet spin state was found to be more stable in even electron structures; the odd electron L-Cu_2OCH_3 and L-Cu_2OH are doublets. L refers to the zeolite lattice. The geometries and zero-point energies of the L-Cu_2O structural models (SI Tables S1, S2) were obtained with the B3LYP functional in constrained optimization with eight Si atoms frozen in their crystal positions.[16] Single-point energies with the M06-2X functional are also listed in SI Table S1.

RESULTS AND DISCUSSION

Catalytic and XAS Measurements. Scheme 1 shows the series of treatments performed on Cu−MOR for converting methane to methanol, which consists of (step 1) drying after catalyst synthesis, (step 2) activation in oxygen, (step 3) reaction with methane, and (step 4) desorption of the methane conversion intermediate either by (step 4a) thermal treatment in dry helium or (step 4b) interaction with a wet helium flow. Figure 1 shows the X-ray absorption near edge structure (XANES) spectra recorded at the key steps of the methane-to-methanol reaction, that is, 1, 2, 3, and 4a in Scheme 1.

The starting Cu−MOR (step 1) is composed of hydrated Cu^{II} sites after wet ion exchange, as seen from our XAS data (Figure 1) and in accordance with literature.[17] The weak pre-edge feature of the XANES at 8977 eV and the localization of the rising edge around 8987 eV are indicative of Cu^{II}. The high intensity of the absorption feature around 8997 eV is characteristic of coordination to water or OH groups. These observations are in agreement with the literature showing that the copper species in Cu-zeolites after aqueous ion exchange and drying at 110 °C are composed mostly of hydrated Cu^{II} sites.[17a]

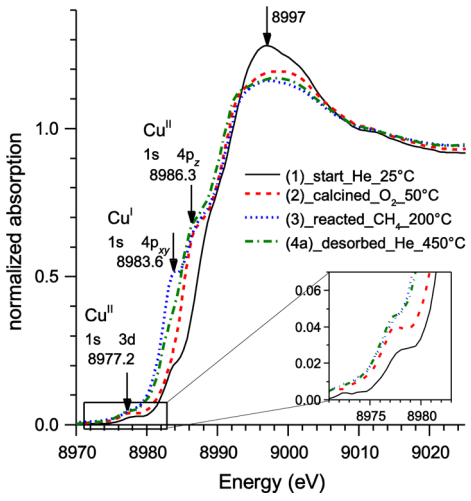

Figure 1. XANES spectra of Cu−MOR recorded at key conditions of the methane conversion reaction as displayed in Scheme 1: starting material (1), calcined in oxygen (2), reacted with methane (3), and after heating in helium (4a) to release the adsorbed intermediate.

After calcination (step 2), the Cu sites loose coordination by dehydration to form oxygenated active Cu^{II} sites. The XANES spectrum of Cu−MOR after calcination (Figure 1) shows an increased intensity of the 8977 eV pre-edge feature and a loss in intensity of the 8997 eV maximum absorption feature. The loss in whiteline intensity is similar to the behavior of $Cu(NO_3)_2$ when water ligands are removed.[18] The XANES spectrum also shows a more prominent rising edge feature to lower energy, which suggests a change of the structure of the Cu sites from $Cu(OH)_2$-like to CuO-like. The FT EXAFS of the spectrum recorded at this step and an XRD diffractogram of calcined Cu−MOR exclude the presence of a significant fraction of large copper oxide clusters, although the presence of additional isolated and oligonuclear Cu^{II} species cannot be excluded (vide infra). The formation of a [Cu^{II}−O_2−Cu^{II}] core resulting from high-temperature treatment in oxygen has been identified before on the basis of the UV−visible spectroscopy and XAS by Groothaert and co-workers.[2a,19] They attributed the UV−vis band at 22700 cm^{-1} measured on Cu-ZSM-5 samples to the O → Cu charge transfer of the bis(μ-oxo)dicopper^{II} species[2a] and later assigned it to a mono(μ-oxo)dicopper^{II} species, [Cu^{II}−O−Cu^{II}], after complementary resonant Raman spectroscopy and DFT calculations.[4a]

The dicopper core in Cu-ZSM-5 was regarded as responsible for converting methane to methanol. On Cu−MOR, however, multiple methane activation sites were proposed because of the discrepancy between the intensity of the UV−vis spectroscopic signature at 22200 cm^{-1} for the copper−oxygen core versus the amount of methanol that can be extracted.[2b] No further investigation has yet been reported on the mechanism at the actual conditions of methanol formation on Cu−MOR. Our UV−vis measurements of the oxygen activated state of Cu−MOR showed a band at 22700 cm^{-1}, in agreement with the results of Groothaert and co-workers.[5a] In addition, literature suggests the presence of isolated Cu^{II} ions, which are indicated by their resistance to autoreduce in He at high temperature.[17d]

A large fraction of the Cu^{II} species react with methane (step 3), undergoing reduction to Cu^{I}.[4c] The XANES recorded after reaction with methane (Figure 1) shows the formation of a distinct feature at 8983.6 eV, which is attributed to the 1s → 4p transition of Cu^{I}.[20] Linear combination fitting of this XANES spectrum (Figure 2) taken after reaction with methane showed contributions of 41% Cu^{I}, 37% Cu^{II} oxide, and 22% hydrated Cu^{II}.

Heating in He(O_2) (step 4a) resulted in the formation of CO_2.[5a] Instead of burning the adsorbed species to CO_2, we were able to desorb it as MeOH by admitting H_2O vapor with 1 ppmv of O_2 at 200 °C (step 4b). Figure 3a shows the MS signals of CO_2, H_2O and MeOH (monitored in the m/z = 31 channel as CH_2OH^+) during the interaction with the wet helium stream at 200 °C directly after methane activation. At the same time that H_2O was observed at the exit of the reactor, the MeOH signal increased, showing high intensity for the first 5 min and a quick decrease afterward. Desorption of MeOH was virtually finished after 20 min. There was no detectable increase in the CO_2 signal during the treatment with water and formation of MeOH.

dx.doi.org/10.1021/cs400713c | ACS Catal. 2014, 4, 16−22

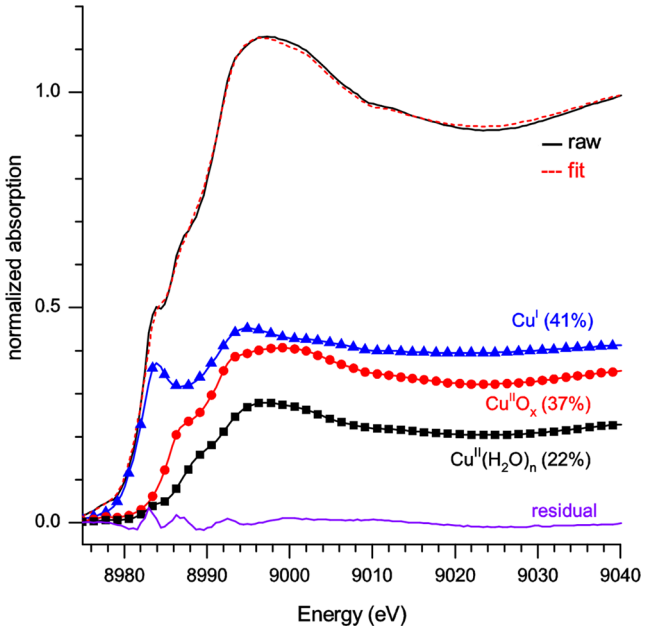

Figure 2. XANES spectrum taken of Cu−MOR during methane interaction at 200 °C with the linear combination fit, its individual components, and the residual from the fit.

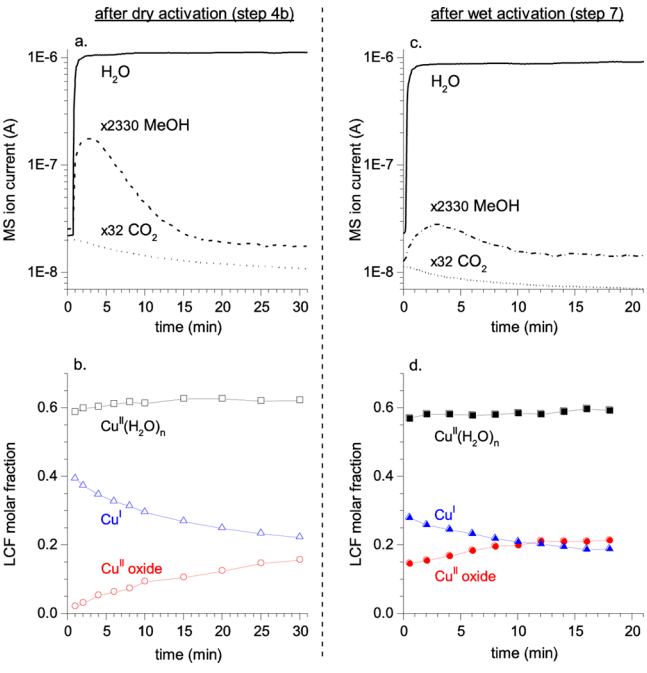

Figure 3. (a) MS profiles of water (——, m/z = 18), MeOH (— —, m/z = 31), and CO_2 (- -, m/z = 44) recorded during interaction with a wet stream of helium at 200 °C after methane interaction (step 4b in Scheme 2); (b) the fit components: Cu^{II}(H$_2$O)$_n$ (–□–), Cu^{I} (blue open triangle), and Cu^{II} oxide (red circle) from the linear combination fit of the XAS spectra recorded at the same time as part a; (c) MS profiles of water, MeOH, and CO_2 recorded during interaction with a wet stream of helium at 200 °C (step 7 in Scheme 2) after pretreatment with wet helium (step 5) and methane interaction at 200 °C (step 6); and (d) the fit components: Cu^{II}(H$_2$O)$_n$ (–■–), Cu^{I} (blue solid triangle), and Cu^{II} oxide (red solid dot) from the linear combination fit of the XAS spectra recorded at the same time as part c.

Figure 4a and 4b show the time-resolved XAS spectra collected during desorption of the methane conversion product

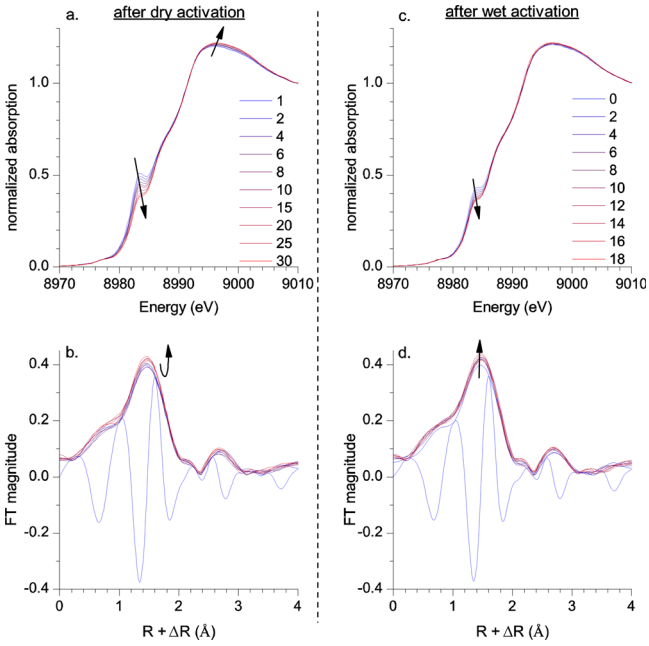

Figure 4. Comparison of the XANES and non-phase-corrected k^3-weighted FT EXAFS spectra taken during desorption of methanol after dry (left) and wet activation (right). For clarity, only the first FT EXAFS spectrum is displayed with an imaginary part. Subsequent FT EXAFS spectra did not display observable changes in their imaginary parts.

by the H_2O/He stream (step 4b in Scheme 1). The XANES series (Figure 4a) showed a substantial decrease in the 8983.6 eV Cu^{I} feature and a small increase in the 8993 eV maximum absorption feature. From the LCF of the spectrum taken at the end of MeOH desorption, we deciphered that Cu was transformed into 62% hydrated Cu^{II}, 22% Cu^{I}, and 16% Cu^{II} oxide (Figure 3b). After desorption of MeOH, heating in He(O_2) provided only a tiny amount of CO_2, indicating that virtually all intermediate was removed as methanol.[5a] The corresponding FT EXAFS (Figure 4b), however, showed only minor changes in the intensity of the first and second coordination shells at around 1.4 and 2.6 Å (R + ΔR), respectively. This suggests that the formation of MeOH is not accompanied by large geometric changes, such as sintering, and that the reaction is limited to the first two coordination shells of Cu. Bound activated methane is associated with Cu^{I} sites, as the 8983.6 eV feature decreases with the time of the desorption of MeOH (Figure 3b, 4a).

The development of Cu species during the H_2O/He treatment, quantified by the LCF (Figure 3b) shows that a further small Cu^{II} oxide contribution forms in the presence of water and accompanies the decrease in the Cu^{I} component. We suggest that this oxygenated Cu^{II} component is different from the well characterized but water-unstable (μ-oxo)dicopper^{II} species, which becomes fully hydrated.[2a] We observed that at least part of this water-stable Cu^{II} oxide is also active for methane conversion. This is demonstrated by the following experiment. Cu−MOR was subjected to the H_2O/He environment (step 5) after high-temperature calcination and subsequently exposed to methane at 200 °C (step 6). Subsequent interaction of the catalyst with H_2O/He (step 7) showed the evolution of MeOH (Figure 3c). The amount of MeOH was about one-tenth of that in the previous experiment (Figure 3a). The in situ XAS after methane activation by wet

dx.doi.org/10.1021/cs400713c | ACS Catal. 2014, 4, 16−22

pretreated Cu−MOR (Figure 5) showed that also in this case, methane activation is accompanied by a reduction of part of the

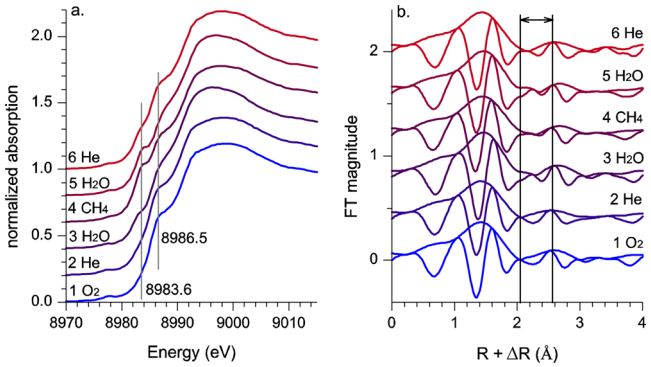

Figure 5. XANES and non-phase-corrected k^3-weighted FT EXAFS spectra of Cu−MOR taken during the wet pretreatment. The vertical lines at 8983.5 and 8986.5 eV identify signatures of Cu^{I} and Cu^{II}, respectively.

Cu^{II} oxide species to Cu^{I}. LCF of the in situ XAS during the evolution of MeOH by the wet pretreated Cu−MOR (Figure 3d) showed behavior similar to that of the dry counterpart, such as a decrease in the amount of the Cu^{I} fraction and an increase in the amount of Cu^{II} oxide.

Discussion and DFT calculations. Scheme 2 shows the evolution of the structure of Cu sites throughout the reaction chain, corresponding to the conditions outlined in Scheme 1 and in agreement with the literature and our experimental and theoretical results. The copper sites in Cu−MOR are in the hydrated state after synthesis by aqueous ion exchange (step 1). These sites are inactive because the saturated coordinative bonds of Cu render the Cu sites unable to further coordinate reactant molecules. High-temperature treatment promotes dehydration and loss of oxygen nearest neighbors. The resulting undercoordinated sites are able to activate molecular oxygen (step 2) to form the oxygenated active site for converting methane to methanol. The literature suggests that the precursor to the active site takes the form of a μ-(η^2:η^2) peroxo dicopper^{II} species $[Cu_2(O_2)]^{2+}$ and that spectator Cu^{I} ions in the zeolite ion-exchange sites provide two electrons to break the peroxo bond and transform the precursor species to a mono(μ-oxo) dicopper^{II} species, which is the active site.[3c]

For a Si/Al ratio between 8 and 12, the shortest distance between dicopper cores is around 7.5 Å, that is, between two consecutive 12-membered rings in MOR. If, during initial oxygen activation, spectator Cu^{I} ions are sufficiently close to provide electrons to the side-on bridged peroxo dicopper^{II} precursor for its conversion to the mono(μ-oxo)dicopper^{II} species, as previously proposed,[3c,9] it is quite likely that these species are also involved in forming stable intermediates to coordinate either H or CH_3 from methane. This will contribute to the formation of a highly stable Cu^{I} species, which is long-lived enough to be detected by XAS. Indeed, during reaction with methane (step 3), the XAS data showed that around half of the Cu^{II} sites reduce to Cu^{I} (41% Cu^{I} and 37% Cu^{II}, and 20% hydrated Cu^{II}) and that a small fraction of Cu^{II} is ligated with either water or OH species. The formation of a significant amount of long-lived Cu^{I} implies that it is a stable species, analogous to the exothermic methane activation mechanism by chemisorption and CH_3 production on $V_4O_{10}^{+}$ clusters.[21]

Scheme 2. Proposed Scheme of Structural Changes of the Active Cu Species in Cu−Mordenite Based on Former Studies, Mass Spectrometry, UV−Visible Spectrometry, Infrared Spectroscopy, and Quick XAS Data[a]

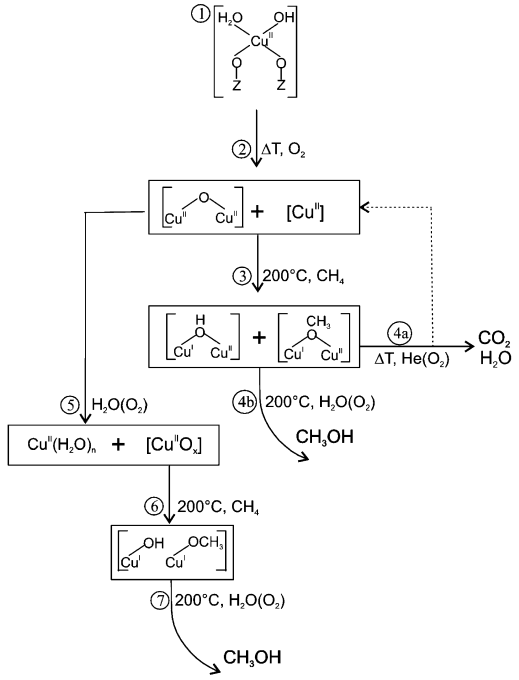

[a]Cu−MOR after aqueous ion exchange (1) is composed of hydrated Cu^{II} sites. Thermal treatment in (dry) oxygen (2) forms the water-sensitive dicopper active sites. Reaction with methane (3) reduces a significant fraction of the copper sites and forms the sorbed reaction intermediate, which may be removed by heating (4a) as CO_2 or by water-assisted desorption (4b) as MeOH. Treatment of oxygen-activated Cu−MOR with water (5) leaves a water-stable Cu^{II} oxide species that activates methane (6−7).

We have found physisorption and chemisorption, however, to be isoenergetic and highly endothermic at [Cu^{II}−O−Cu^{II}] sites,[4a,9] which suggests that a mechanism other than that proposed by Woertink and co-workers[4a] is at work. Contrary to the formation of the cupric−oxyl [Cu^{I}−$OHCH_3$−Cu^{II}] species as the activated methane intermediate, and having observed that around half of the total Cu sites reduce to Cu^{I} after reaction with methane, we infer that a methoxy species is bound to a mixed-valent dicopper site, [Cu^{I}−OCH_3−Cu^{II}], whereas the abstracted H atom from methane resides as hydroxyl between immediate neighboring Cu^{I} and Cu^{II} sites. When the C−H bond is cleaved, two stable [Cu^{I}−OCH_3−Cu^{II}] and [Cu^{I}−OH−Cu^{II}] complexes are formed. Our DFT calculations on the same L-Cu_2O model site as proposed by Woertink et al.[4a] predicted that the chemisorbed structure is stabilized by 60 kcal mol^{-1} when the methyl binds to another [Cu^{II}−O−Cu^{II}] species to form [Cu^{I}−OCH_3−Cu^{II}] and [Cu^{I}−OH−Cu^{II}], making methane activation exothermic by 50 kcal mol^{-1} (Figure 6), in contrast to the endothermic formation of [Cu^{I}−$OHCH_3$−Cu^{II}].[4a] We also investigated the binding energy of H and CH_3 to a bridging oxygen in the zeolite framework and found it to be 38 and 40 kcal mol^{-1} lower than the binding energy to the [Cu^{II}−O−Cu^{II}] species, respectively (B3LYP/6-311+G(d) results). Therefore, H and CH_3 are unlikely to coordinate to the zeolite framework and form stable structures.

dx.doi.org/10.1021/cs400713c | ACS Catal. 2014, 4, 16−22

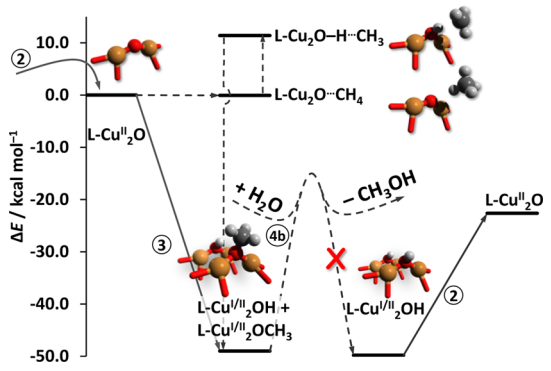

Figure 6. B3LYP/6-311+G(d) energy diagram for the dicopper active site L-Cu_2O in the methane-to-methanol conversion. Solid arrows indicate processes supported by experimental and computational evidence. The presumably short-lived physi- and chemisorbed intermediates are not observed experimentally, and no transition state or final product is reported for $Cu_2O–CH_3$ hydrolysis. The catalytic cycle is stopped by the irreversible hydration of the active L-Cu_2O site after methanol desorption.

Introduction of moisture allows desorption of the intermediate as MeOH (step 4b), and the XAS analysis of the spectra recorded simultaneously showed that the methane conversion intermediate is associated with a Cu^I species. The hydrolysis of $[Cu^I–OCH_3–Cu^{II}]$ to form methanol may proceed through a ring $[Cu_2O···H···OH···CH_3]$ transition state, possibly mediated by Cu^I, and is driven by excess H_2O and a moderate exothermicity of 1 kcal mol^{-1} (Figure 6). The weak $O–CH_3$ bond at the [Cu–O–Cu] site ($BE_{O–H}$, 87.3 > $BE_{O–CH_3}$, 62.8 kcal/mol) enables MeOH to desorb and makes the hydrolysis entropically favored. XAS analysis further showed that there exists a water-stable Cu^{II} oxide species that is also able to activate methane and form methanol. It is possible that the water-stable species is able to sustain a reversible hydration–dehydration at 200 °C or that it is able to resist total hydration. Although the structure of the water-stable sites is not known, the energetics of the partial methane oxidation pathway is expected to be similar to that shown in Figure 6 if the site allows for the formation of $[Cu_2OH]$ and $[Cu_2OCH_3]$ intermediates.

Implications. Two important observations suggest that it may be possible to operate this low-temperature methane-to-methanol process in batch mode. The first is the reoxidation of Cu^I to Cu^{II} in the presence of tiny concentrations of O_2 (contained in the He gas) at moderate temperatures (<200 °C). This means that high-temperature treatment might not be necessary to reactivate the Cu sites for the next turnover. The second is the formation of a Cu^{II} oxide species that is not hydrated at 200 °C in the presence of water and oxygen. At least part of this species activates methane. Methanol was formed during the $H_2O(O_2)$-desorption treatment after hydration and methane activation. Its amount was less than that observed upon dry activation via the mono(μ-oxo)-dicopper species; nevertheless, this experiment shows that an active Cu^{II} oxide species resists total hydration.

These observations imply that the structure of the active Cu sites is a dynamic function of the reaction conditions. In a dry environment, the Cu sites take the form of dehydrated Cu^{II} oxide, which corresponds to the well-characterized mono(μ-oxo)dicopper^{II} species, responsible for the production of CO_2 or MeOH, depending on the conditions. In wet conditions, the mono(μ-oxo)dicopper^{II} species are destabilized, but a small amount of water-stable Cu^{II} oxide is active for methane activation. Given that a feasible catalytic cycle has to operate in a hydrated environment because of the necessity to desorb the intermediate, investigating the nature of the water-stable Cu^{II} oxide sites promises perhaps even bigger strides toward low-temperature methane partial oxidation.

CONCLUSIONS

A large fraction of oxygen-activated Cu^{II} reacts with methane to reduce to Cu^I and to contain the adsorbed methane conversion intermediate. On the basis of density functional theory calculations, $[Cu^I–OCH_3–Cu^{II}]$ and $[Cu^I–OH–Cu^{II}]$ are proposed as plausible structures for the adsorbed intermediates.

At least two types of Cu^{II} sites were identified as active for converting methane to methanol, depending on the reaction conditions. In addition to the characterized but water-unstable mono(μ-oxo) and bis(μ-oxo) dicopper species, a fraction of active Cu^{II} survives total hydration to provide a water-stable Cu^{II} oxide species that also activates methane.

ASSOCIATED CONTENT

Supporting Information

Additional experimental details and data. This material is available free of charge via the Internet at http://pubs.acs.org.

AUTHOR INFORMATION

Corresponding Author

*E-mail: j.a.vanbokhoven@chem.ethz.ch.

Notes

The authors declare no competing financial interest.

REFERENCES

(1) (a) Holmen, A. *Catal. Today* **2009**, *142* (1–2), 2–8. (b) Schwarz, H. *Angew. Chem., Int. Ed.* **2011**, *50* (43), 10096–10115. (c) Alvarez-Galvan, M. C.; Mota, N.; Ojeda, M.; Rojas, S.; Navarro, R. M.; Fierro, J. L. G. *Catal. Today* **2011**, *171* (1), 15–23.

(2) (a) Groothaert, M. H.; Smeets, P. J.; Sels, B. F.; Jacobs, P. A.; Schoonheydt, R. A. *J. Am. Chem. Soc.* **2005**, *127* (5), 1394–1395. (b) Smeets, P. J.; Groothaert, M. H.; Schoonheydt, R. A. *Catal. Today* **2005**, *110* (3–4), 303–309.

(3) (a) Yumura, T.; Takeuchi, M.; Kobayashi, H.; Kuroda, Y. *Inorg. Chem.* **2009**, *48* (2), 508–517. (b) Itadani, A.; Sugiyama, H.; Tanaka, M.; Ohkubo, T.; Yumura, T.; Kobayashi, H.; Kuroda, Y. *J. Phys. Chem. C* **2009**, *113* (17), 7213–7222. (c) Smeets, P. J.; Hadt, R. G.; Woertink, J. S.; Vanelderen, P.; Schoonheydt, R. A.; Sels, B. F.; Solomon, E. I. *J. Am. Chem. Soc.* **2010**, *132* (42), 14736–14738. (d) Ene, A. B.; Bauer, M.; Archipov, T.; Roduner, E. *Phys. Chem. Chem. Phys.* **2010**, *12* (24), 6520–6531. (e) Dietl, N.; van der Linde, C.; Schlangen, M.; Beyer, M. K.; Schwarz, H. *Angew. Chem., Int. Ed.* **2011**, *50* (21), 4966–4969.

(4) (a) Woertink, J. S.; Smeets, P. J.; Groothaert, M. H.; Vance, M. A.; Sels, B. F.; Schoonheydt, R. A.; Solomon, E. I. *Proc. Natl. Acad. Sci. U.S.A.* **2009**, *106* (45), 18908–18913. (b) Beznis, N. V.; Weckhuysen, B. M.; Bitter, J. H. *Catal. Lett.* **2010**, *138* (1–2), 14–22. (c) Alayon, E. M. C.; Nachtegaal, M.; Kleymenov, E.; van Bokhoven, J. A. *Microporous Mesoporous Mater.* **2013**, *166* (0), 131–136.

(5) (a) Alayon, E. M.; Nachtegaal, M.; Ranocchiari, M.; van Bokhoven, J. A. *Chem. Commun.* **2012**, *48* (3), 404–406. (b) Hammond, C.; Forde, M. M.; Ab Rahim, M. H.; Thetford, A.; He, Q.; Jenkins, R. L.; Dimitratos, N.; Lopez-Sanchez, J. A.; Dummer, N. F.; Murphy, D. M.; Carley, A. F.; Taylor, S. H.; Willock, D. J.; Stangland, E. E.; Kang, J.; Hagen, H.; Kiely, C. J.; Hutchings, G. J. *Angew. Chem., Int. Ed.* **2012**, *51* (21), 5129–5133.

(6) Kurnaz, E.; Fellah, M. F.; Onal, I. *Microporous Mesoporous Mater.* **2011**, *138* (1−3), 68−74.
(7) (a) Shilov, A. E.; Shteinman, A. A. *Russ. Chem. Rev.* **2012**, *81* (4), 291−316. (b) Hammond, C.; Conrad, S.; Hermans, I. *ChemSusChem* **2012**, *5* (9), 1668−86. (c) Vanelderen, P.; Vancauwenbergh, J.; Sels, B. F.; Schoonheydt, R. A. *Coord. Chem. Rev.* **2013**, *257* (2), 483−494.
(8) (a) Chen, P. P. Y.; Yang, R. B. G.; Lee, J. C. M.; Chan, S. I. *Proc. Natl. Acad. Sci. U.S.A.* **2007**, *104* (37), 14570−14575. (b) Balasubramanian, R.; Smith, S. M.; Rawat, S.; Yatsunyk, L. A.; Stemmler, T. L.; Rosenzweig, A. C. *Nature* **2010**, *465* (7294), 115−U131.
(9) Vanelderen, P.; Hadt, R. G.; Smeets, P. J.; Solomon, E. I.; Schoonheydt, R. A.; Sels, B. F. *J. Catal.* **2011**, *284* (2), 157−164.
(10) (a) Singh, J.; Lamberti, C.; van Bokhoven, J. A. *Chem. Soc. Rev.* **2010**, *39* (12), 4754−4766. (b) Bordiga, S.; Bonino, F.; Lillerud, K. P.; Lamberti, C. *Chem. Soc. Rev.* **2010**, *39* (12), 4885−4927. (c) Bordiga, S.; Groppo, E.; Agostini, G.; Van Bokhoven, J. A.; Lamberti, C. *Chem. Rev.* **2013**, *113*, 1736−1850. (d) Giordanino, F.; Vennestrom, P. N. R.; Lundegaard, L. F.; Stappen, F. N.; Mossin, S.; Beato, P.; Bordiga, S.; Lamberti, C. *Dalton Trans.* **2013**, *42*, 12741−12761.
(11) (a) Hämäläinen, K.; Siddons, D. P.; Hastings, J. B.; Berman, L. E. *Phys. Rev. Lett.* **1991**, *67* (20), 2850−2853. (b) Safonova, O. V.; Tromp, M.; van Bokhoven, J. A.; de Groot, F. M. F.; Evans, J.; Glatzel, P. *J. Phys. Chem. B* **2006**, *110* (33), 16162−16164.
(12) Frahm, R.; Nachtegaal, M.; Stotzel, J.; Harfouche, M.; van Bokhoven, J. A.; Grunwaldt, J. D. *AIP Conference Proceedings* **2010**, *1234*, 251−255.
(13) Vaarkamp, M.; Linders, J. C.; Koningsberger, D. C. *Physica B* **1995**, *208 & 209*, 159−60.
(14) Ravel, B.; Newville, M. *J. Synchroton Radiat.* **2005**, *12*, 537−541.
(15) Frisch, M. J.; Trucks, G. W.; Schlegel, H. B.; Scuseria, G. E.; Robb, M. A.; Cheeseman, J. R.; Scalmani, G.; Barone, V.; Mennucci, B.; Petersson, G. A.; Nakatsuji, H.; Caricato, M.; Li, X.; Hratchian, H. P.; Izmaylov, A. F.; Bloino, J.; Zheng, G.; Sonnenberg, J. L.; Hada, M.; Ehara, M.; Toyota, K.; Fukuda, R.; Hasegawa, J.; Ishida, M.; Nakajima, T.; Honda, Y.; Kitao, O.; Nakai, H.; Vreven, T.; Montgomery, J. A.; Peralta, J. E.; Ogliaro, F.; Bearpark, M.; Heyd, J. J.; Brothers, E.; Kudin, K. N.; Staroverov, V. N.; Kobayashi, R.; Normand, J.; Raghavachari, K.; Rendell, A.; Burant, J. C.; Iyengar, S. S.; Tomasi, J.; Cossi, M.; Rega, N.; Millam, J. M.; Klene, M.; Knox, J. E.; Cross, J. B.; Bakken, V.; Adamo, C.; Jaramillo, J.; Gomperts, R.; Stratmann, R. E.; Yazyev, O.; Austin, A. J.; Cammi, R.; Pomelli, C.; Ochterski, J. W.; Martin, R. L.; Morokuma, K.; Zakrzewski, V. G.; Voth, G. A.; Salvador, P.; Dannenberg, J. J.; Dapprich, S.; Daniels, A. D.; Farkas; Foresman, J. B.; Ortiz, J. V.; Cioslowski, J.; Fox., D. J. *Gaussian 09*; Gaussian, Inc.: Wallingford, CT, 2010.
(16) Olson, D. H.; Kokotailo, G. T.; Lawton, S. L.; Meier, W. M. *J. Phys. Chem.* **1981**, *85* (15), 2238−2243.
(17) (a) Larsen, S. C.; Aylor, A.; Bell, A. T.; Reimer, J. A. *J. Phys. Chem.* **1994**, *98* (44), 11533−11540. (b) Lo Jacono, M.; Fierro, G.; Dragone, R.; Feng, X. B.; d'Itri, J.; Hall, W. K. *J. Phys. Chem. B* **1997**, *101* (11), 1979−1984. (c) Dedecek, J.; Wichterlova, B. *J. Phys. Chem. B* **1997**, *101* (49), 10233−10240. (d) Palomino, G. T.; Bordiga, S.; Zecchina, A.; Marra, G. L.; Lamberti, C. *J. Phys. Chem. B* **2000**, *104*, 8641−8651. (e) Llabrés i Xamena, F. X.; Fisicaro, P.; Berlier, G.; Zecchina, A.; Turnes Palomino, G.; Prestipino, C.; Bordiga, S.; Giamello, E.; Lamberti, C. *J. Phys. Chem. B* **2003**, *107* (29), 7036−7044.
(18) Cheng, N.; Wei, Y. L.; Yang, Y. W.; Lee, J. F. *Phys. Scr.* **2005**, *T115*, 907−908.
(19) Groothaert, M. H.; van Bokhoven, J. A.; Battiston, A. A.; Weckhuysen, B. M.; Schoonheydt, R. A. *J. Am. Chem. Soc.* **2003**, *125* (25), 7629−7640.
(20) (a) Tranquada, J. M.; Heald, S. M.; Moodenbaugh, A. R. *Phys. Rev. B* **1987**, *36* (10), 5263−5274. (b) Kau, L. S.; Spirasolomon, D. J.; Pennerhahn, J. E.; Hodgson, K. O.; Solomon, E. I. *J. Am. Chem. Soc.* **1987**, *109* (21), 6433−6442. (c) Prestipino, C.; Berlier, G.; Xamena, F. X. L. I.; Spoto, G.; Bordiga, S.; Zecchina, A.; Palomino, G. T.; Yamamoto, T.; Lamberti, C. *Chem. Phys. Lett.* **2002**, *363*, 389−396.
(21) Feyel, S.; Doebler, J.; Schroeder, D.; Sauer, J.; Schwarz, H. *Angew. Chem., Int. Ed.* **2006**, *45* (28), 4681−4685.